THE JOURNAL OF BIOLOGICAL CHEMISTRY VOL. 283, NO. 39, pp. 26490–26498, September 26, 2008

Structure and Biochemical Properties of Fission Yeast Arp2/3 Complex Lacking the Arp2 Subunit*[S]

Received for publication, April 3, 2008, and in revised form, June 17, 2008 Published, JBC Papers in Press, July 18, 2008, DOI 10.1074/jbc.M802607200

Brad J. Nolen[1] **and Thomas D. Pollard**

From the Departments of Molecular, Cellular and Developmental Biology, Cell Biology, and Molecular Biophysics and Biochemistry, Yale University, New Haven, Connecticut 06520-8103

Arp2/3 (actin-related protein 2/3) complex is a seven-subunit complex that nucleates branched actin filaments in response to cellular signals. Nucleation-promoting factors such as WASp/Scar family proteins activate the complex by facilitating the activating conformational change and recruiting the first actin monomer for the daughter branch. Here we address the role of the Arp2 subunit in the function of Arp2/3 complex by isolating a version of the complex lacking Arp2 (Arp2Δ Arp2/3 complex) from fission yeast. An x-ray crystal structure of the ΔArp2 Arp2/3 complex showed that the rest of the complex is unperturbed by the loss of Arp2. However, the Arp2Δ Arp2/3 complex was inactive in actin nucleation assays, indicating that Arp2 is essential to form a branch. A fluorescence anisotropy assay showed that Arp2 does not contribute to the affinity of the complex for Wsp1-VCA, a *Schizosaccharomyces pombe* nucleation-promoting factor protein. Fluorescence resonance energy transfer experiments showed that the loss of Arp2 does not prevent VCA from recruiting an actin monomer to the complex. Truncation of the N terminus of ARPC5, the smallest subunit in the complex, increased the yield of Arp2Δ Arp2/3 complex during purification but did not compromise nucleation activity of the full Arp2/3 complex.

Dynamic rearrangements of the actin cytoskeleton are essential for cellular responses to the environment, and cells employ a host of proteins to control nucleation, polymerization, capping, severing, bundling, cross-linking, and depolymerization of actin (1). Fission yeast have two well characterized nucleators of actin filaments, formins (Cdc12 and For3) and Arp2/3 complex (consisting of seven-subunits, Arp3, Arp2, and ARPC1–5) (2). Formins assemble unbranched filaments present both in cables that span the length of interphase cells and in the contractile ring, which constricts during cytokinesis (3, 4). Arp2/3 complex nucleates branched filaments in cortical structures called actin patches, which are sites of endocytosis located at cell poles during interphase and the cleavage furrow during cytokinesis (5–7).

Arp2/3 complex nucleates actin filament branches on the sides of pre-existing (mother) filaments (8). The new (daughter) filament grows at an angle of 78° on the side of the mother filament (9). Arp2/3 complex from most species is intrinsically inactive but is stimulated to form an actin filament branch through interactions with proteins called nucleation promoting factors (NPFs),[2] ATP, an actin monomer, and the side of a mother filament (2). WASp/Scar family proteins, the prototypical NPFs, contain a C-terminal region termed VCA (verprolin homology, central, acidic), which is the minimal fragment required to activate nucleation by Arp2/3 complex. Crystallographic and electron microscopic data suggest that a conformational change reorients the two actin-related subunits, Arp2 and Arp3, like two successive actin subunits along the short pitch helix of an actin filament to create the nucleus for polymerization of the daughter filament (9, 10). A model built by fitting crystal structures into reconstructions of electron tomograms of branch junctions shows that all seven subunits of Arp2/3 complex contact the mother filament and that the barbed ends of Arp2 and Arp3 interact with the pointed end of the daughter filament (9).

Numerous questions remain about the mechanism of branching nucleation despite many structural and kinetic studies. Nucleotide binding favors a conformation of Arp3 that may contribute to activation (11, 12). The V region of NPFs binds an actin monomer (13, 14), recruiting it to the branch point, whereas the C and A regions bind to Arp2/3 complex and are thought to facilitate conformational changes required for nucleation (14, 15). Cross-linking, radiation footprinting, and NMR experiments have implicated all but two subunits (ARPC2 and ARPC4) in interactions with VCA (16–19), but no high resolution structural information on VCA binding is available. A model based on small angle x-ray scattering of Arp2/3 complex bound to actin and VCA has the actin monomer located at the barbed end of Arp2 (20). Expression of recombinant human Arp2/3 complex subunits in insect cells demonstrated that ARPC2 and ARPC4 are essential for the integrity of the complex and that both of these subunits and Arp3 are necessary to assemble a complex that can nucleate actin filaments

* This work was supported, in whole or in part, by National Institutes of Health Grant GM066311. This work was also supported by National Institutes of Health Ruth Kirschstein postdoctoral fellowship GM074374-02. The costs of publication of this article were defrayed in part by the payment of page charges. This article must therefore be hereby marked "*advertisement*" in accordance with 18 U.S.C. Section 1734 solely to indicate this fact.

The atomic coordinates and structure factors (code 3DWL) have been deposited in the Protein Data Bank, Research Collaboratory for Structural Bioinformatics, Rutgers University, New Brunswick, NJ (http://www.rcsb.org/).

[S] The on-line version of this article (available at http://www.jbc.org) contains supplemental text and Figs. S1–S4.

[1] To whom correspondence should be addressed: Tel.: 203-432-3194; Fax: 203-432-6161; E-mail: bradley.nolen@yale.edu.

[2] The abbreviations used are: NPF, nucleation promoting factor; DTT, dithiothreitol; GST, glutathione *S*-transferase; OG-actin, Oregon Green-actin; FRET, fluorescence resonance energy transfer; YFP, yellow fluorescent protein; CFP, cyan fluorescent protein.

(21). This study did not address the role of Arp2 in the stability and nucleation activity of Arp2/3 complex.

Here, we show that a complex lacking the Arp2 subunit (ΔArp2 Arp2/3 complex) can be isolated from fission yeast. Except for the absence of Arp2, the loss of Arp2 did not perturb the crystal structure of Arp2/3 complex. ΔArp2 Arp2/3 complex bound Wsp1-VCA but did not nucleate actin filaments, so Arp2 is essential to initiate a branch. Mutational analysis showed that branching nucleation does not require the N terminus of ARPC5 to anchor Arp2 as proposed in one model of activation (22).

EXPERIMENTAL PROCEDURES

Purification of S. pombe Arp2/3 Complex—We purified native Arp2/3 complex from *Schizosaccharomyces pombe* strain TM011 typically starting with 500 g of wet cells. Ten milliliters of a turbid culture of cells was inoculated per liter of media made from 35 g/liter YES (Q-biogene) and grown with vigorous shaking overnight at 30 °C. In the morning, an additional 70 g/liter YES was added, and the cultures were grown to an optical density of ~6.0 at 600 nm. Cells were then pelleted and washed in lysis buffer (20 mM Tris, pH 8.0, 50 mM NaCl, and 1 mM EDTA). Pellets of cells were resuspended in 1 ml of lysis buffer per gram of wet cells and stored at −80 °C until lysis. After thawing, an additional 0.4 ml of lysis buffer plus DTT (to 1 mM) and Complete protease inhibitor tablets (Roche Applied Science, 1 tablet per 50 ml) were added per gram of cells. All subsequent steps were at 0–4 °C. Cells were lysed using a Microfluidizer (Microfluidics, model 110EH). Phenylmethylsulfonyl fluoride was added to 1 mM, and the lysate was centrifuged at 30,000 × *g* for 20 min. The supernatant was centrifuged a second time at 125,000 × *g* for 1 h, filtered through cheesecloth, and loaded onto a 150-ml Q-Sepharose column equilibrated with lysis buffer. The column was washed with 1.5 column volumes of lysis buffer containing 1 mM DTT, and protein eluted with 20 mM Tris, pH 8.0, 300 mM NaCl, 1 mM EDTA, 1 mM DTT. Protein was precipitated from the eluted fractions with 40% ammonium sulfate, pelleted, and resuspended in 50 ml of PKME (25 mM PIPES, pH 7.0, 50 mM KCl, 1 mM EGTA, 3 mM $MgCl_2$, 1 mM DTT, and 0.1 mM ATP) and dialyzed overnight against the same buffer. The sample was then loaded onto an 8-ml column of glutathione-Sepharose 4B (GE Healthcare) pre-charged with GST-N-WASp-VCA and equilibrated with PKME. GST-N-WASp-VCA was purified as described for GST-WASp-VCA (23). Arp2/3 complex was eluted with a linear 60-ml gradient of 50–1000 mM NaCl. Peak fractions were pooled and dialyzed against 20 mM Tris, pH 8.0, 100 mM NaCl, 1 mM EGTA, 1 mM DTT, and 1 mM $MgCl_2$ and fractionated on a 0.5- × 5-cm column of Mono Q (GE Healthcare) equilibrated with 20 mM Tris, pH 8.0, 100 mM NaCl, 1 mM EGTA, 1 mM DTT, and 1 mM $MgCl_2$ and eluted with a linear 20-ml gradient of 100–400 mM NaCl. Pooled fractions were concentrated to 1.0 ml with Amicon Ultra-15 concentrators (Millipore) and loaded onto a Superdex 200 HR16/60 gel-filtration column (GE Healthcare) equilibrated with 20 mM Tris, pH 8.0, 100 mM NaCl, and 1 mM DTT. Peak fractions were pooled and diluted 2-fold with 20 mM Tris, pH 8.0, and 1 mM DTT before concentrating and flash freezing in liquid nitrogen. Protein concentration was determined by measuring absorbance at 280 nm with extinction coefficients determined by the Von Hippel method (24).

Purification of S. pombe Wsp1-VCA Constructs—pGV67-Wsp1-VCA was constructed by amplifying *S. pombe* Wsp1 residues 497–574 with 5′-BamHI and 3′-EcoRI restriction sites and cloning into pGV67, a plasmid derived from p21d (Novagen) and containing an N-terminal glutathione *S*-transferase (GST) tag followed by a tobacco etch virus cleavage site. pGV67-Wsp1-Cys-VCA was constructed using the same procedure, with a single cysteine inserted 5′ to the 497–574 fragment.

Escherichia coli strain BL21(DE3) was transformed with either pGV67-Wsp1-VCA or pGV67-Wsp1-Cys-VCA, grown to $A_{600\ nm}$ of 0.8, and induced with 0.4 mM isopropyl 1-thio-β-D-galactopyranoside for overnight expression at 22 °C. Cells from an 8-liter culture were harvested and lysed in 300 ml of 20 mM Tris, pH 8.0, 25 mM NaCl, 2 mM DTT, and 1 mM phenylmethylsulfonyl fluoride containing four protease inhibitor tablets (Roche Applied Science) per 50 ml. Cells were lysed with a Branson sonicator, and the lysate was cleared by centrifugation at 100,000 × *g* for 30 min. Supernatant was loaded onto a 35-ml column DEAE-Sepharose equilibrated in lysis buffer and eluted with a linear 300-ml gradient of 25–700 mM NaCl. Fractions containing recombinant protein were pooled and diluted with lysis buffer lacking NaCl to reduce the salt to 140 mM. The sample was then loaded onto a 10-ml column of glutathione-Sepharose 4B equilibrated with 20 mM Tris, pH 8.0, 140 mM NaCl, 2 mM EDTA, and 2 mM DTT (binding buffer) and washed with 5 column volumes of the same buffer. The wash buffer was allowed to drain to the top of the column bed, and 30 μl of 75 μM tobacco etch virus protease (purified from *E. coli* by expression from the pRK1043 tobacco etch virus vector kindly provided by D. Waugh (25)) was mixed into the glutathione-Sepharose slurry. Protein was released from the column during incubation with gentle rocking overnight at 4 °C. Eluted protein was pooled and loaded onto a 0.5- × 5-cm Mono Q column equilibrated with 20 mM Tris, pH 8.0, 100 mM NaCl, and 2 mM DTT. Protein was eluted with a 20-ml linear gradient of 100–800 mM NaCl, concentrated, and purified by size-exclusion chromatography onto a Superdex 75 HR16/60 column (GE Healthcare) in 20 mM Tris, pH 8.0, 100 mM NaCl, and 1 mM DTT before re-concentrating and flash freezing in liquid nitrogen.

Preparation of Rhodamine-labeled Sp-Wsp1-Cys-VCA—Sp-Wsp1-Cys-VCA was purified as the SpWsp1-VCA construct, except that DTT was excluded from the final gel filtration buffer. A fresh 20 mM stock of tetramethylrhodamine-6-maleimide (Invitrogen) in dimethylformamide was added dropwise to the pooled peak fractions of Sp-Wsp1-Cys-VCA while stirring on ice. Reaction was stopped after 1 h by the addition of 1 mM DTT. Labeled protein was separated from free dye by ion-exchange chromatography on a 0.5- × 5-cm Mono Q column and through repeated concentration and dilution in an Amicon Ultra protein concentrator. Concentration of SpWsp1-Rho-VCA (Rho-VCA) was determined by measuring absorbance at 552 nm with an extinction coefficient of 44,660 $M^{-1}cm^{-1}$ (14).

Preparation of Labeled and Unlabeled and Actin Monomers—We purified actin by established procedures: chicken skeletal muscle actin (26), pyrene-labeled actin (27), and Oregon Green-actin (OG-actin) (28).

Construction of Mutant Strains of S. pombe—We constructed mutant strains by PCR-based gene targeting (29). For *ARPC5* mutants, cassettes containing a KanMX6 module and the P3nmt1 thymine-repressible promoter were amplified with long primers to generate a 5′-flanking sequence complimentary to a region 330 nucleotides upstream from the *ARPC5* start codon. The 3′-flanking sequence was complimentary to either the first 60 nucleotides of the *ARPC5* coding region (with codon 3 mutated to change arginine to glutamic acid) or to a region 42 nucleotides downstream from the start codon (for *ARPC5*Δ*N*). Cassettes were transformed into the TM011 strain of *S. pombe* using the lithium acetate method (29, 30). Transformed cells were plated on YES plates and incubated for ~18 h at 30 °C before replica plating onto YES plates containing 100 mg/liter G418/Geneticin (Invitrogen). Replica plates were incubated for 2–3 days, and large colonies were re-streaked on fresh YES plates. Genomic DNA was isolated from mutant strains (29), and the junctions and the entire coding region of *ARPC5* were sequenced to verify the presence of the mutations. *ARPC3-YFP* and *arp2-CFP* strains were provided by Chris Beltzner, and were constructed by replacing the *ARPC3* or *arp2* stop codon in FY527 (*h*$^-$ *leu1–32 ura4-D18 his3-D1 ade6-M216*) or FY528 (*h*$^+$ *leu1–32 ura4-D18 his3-D1 ade6-M210*) with a pFA6a-YFP-kanMX6 or pFA6a-CFP-kanMX6 cassette, crossing, and analyzing tetrads.

Fluorescence Anisotropy Assays—We used an Alphascan fluorometer with a T-format for fluorescence measurements (Photon Technology International). Samples were excited at 552 nm, and anisotropy was measured at 578 nm. The excitation monochromometer bandwidth was 6 nm, and the emission bandwidth was 4 nm. Fixed concentrations of Rho-VCA were titrated with SpArp2/3 complex, and the fluorescence was measured for both filter positions at 0.1 points/s for 40 s. Photon Technology International Felix software was used for data collection and to calculate average anisotropy. For FRET measurements fixed concentrations of OG-actin were titrated with Rho-VCA with excitation at 480 nm, emission at 517 nm, and 3 nm slit widths.

Actin Polymerization Assays—We measured the nucleation activity of wild-type and mutant Arp2/3 complex from the time course of actin polymerization. Polymerization reactions of 100 μl were assembled as follows: 2 μl of 10 mM EGTA and 1 mM $MgCl_2$ were added to 20 μl of 20 μM 15% pyrene actin monomers in G-buffer (2 mM Tris-HCl, pH 8.0, 0.2 mM ATP, 0.1 mM $CaCl_2$, 0.5 mM DTT, and 0.01% NaN_3) followed immediately by adding 78 μl of a solution containing Arp2/3 complex, SpWsp1-VCA with buffers, and salts to bring the final reaction conditions to 10 mM imidazole, pH 7.0, 50 mM KCl, 1 mM EGTA, 1 mM $MgCl_2$. Fluorescence measurements were made at 15-s intervals in a 96-well plate using a Gemini XPS spectrofluorometer (Molecular Devices) with an excitation wavelength of 365 nm and an emission wavelength of 407 nM. The rate of polymerization was determined from the slope of the polymerization curve at 50% polymer formation. The concentration of barbed ends was calculated by setting the rate of polymer formation equal to k_+[ends][actin monomer], where $k_+ = 10$ $\mu M^{-1}s^{-1}$ and solving for [ends].

Determination of Equilibrium Binding Constants—Binding constants were determined by fitting the anisotropy curves to Equation 1,

$$r = rf + (rb - rf)\left(\frac{(K_d + [R] + [L]) - \sqrt{(K_d + [R] + [L])^2 - 4[R][L]}}{2[L]}\right) \quad \text{(Eq. 1)}$$

where *rf* is the signal of the free receptor (*R*), *rb* is the signal of the bound receptor, and [*L*] is the total concentration of the ligand (species titrated). *rb* and K_d were fit using KaleidaGraph (Synergy Software). Determination of binding constants for unlabeled SpWsp1-VCA measured using competition assay is described in the supplemental materials.

Crystal Growth and Structure Determination—Crystals of ΔArp2 Arp2/3 complex grew in 750 mM ammonium sulfate, 50 mM sodium citrate, and 7% glycerol at 4 °C to an average size of 150 × 80 × 80 μm. ATP and calcium chloride were present in the crystallization drop at 0.5 mM each. The crystals diffracted weakly and were indexed to the $P4_222$ space group with a large unit cell (a = 219.1 Å, b = 219.1 Å, c = 315.2 Å) and two molecules in the asymmetric unit (76% solvent). Attempts to dehydrate crystals by increasing the precipitant concentration did not improve diffraction. We used a homology model of the *S. pombe* Arp2/3 complex based on the crystal structure of bovine Arp2/3 complex (31) with the Arp2 subunit removed as a molecular replacement search model. We also removed inserts and regions with high *B*-factors in the bovine complex structure from the search model. We found one solution using the program Phaser (32) with a translational Z-score of 25.6. The initial model was improved through three successive rounds of rebuilding and restrained refinement carried out using REFMAC with a weighting parameter of 0.005. *B*-factors were refined by TLS refinement using one TLS group for each subunit (33). The two molecules in the asymmetric unit were symmetrically constrained throughout the refinement. To improve density for model building, *B*-factors were sharpened using a value of 70 Å^2. The final model had an R_{free} of 34.4% and an R_{work} of 32.4%. Coordinates were deposited in the Protein Data Bank with accession code 3DWL.

Fluorescence Microscopy—Cells were grown to $A_{595} = 0.2$–0.5 in YE5S at 25 °C and washed in Edinburgh minimal medium (potassium phthalate (3 g/liter), Na_2SO_4 (0.04 g/liter), $ZnSO_4$ (0.4 mg/liter), Na_2HPO_4 (2.2 g/liter), pantothenic acid (1 mg/liter), $FeCl_2$ (0.2 mg/liter), NH_4Cl (5 g/liter), nicotinic acid (10 mg/liter), molybdic acid (40 μg/liter), dextrose (20 g/liter), myo-inositol (10 mg/liter), potassium iodide (0.1 mg/liter), $MgCl_2$ (1.05 g/liter), biotin (1 mg/liter), $CuSO_4$ (40 μg/liter), $CaCl_2$ (14.7 mg/liter), boric acid (0.5 mg/liter), citric acid (1 mg/liter), KCl (1 g/liter), $MnSO_4$ (0.4 mg/liter)) before mounting on 25% gelatin pads (34). Images were acquired on an UltraView RS (PerkinElmer Life Sciences) spinning disk confocal system installed on an Olympus IX-71

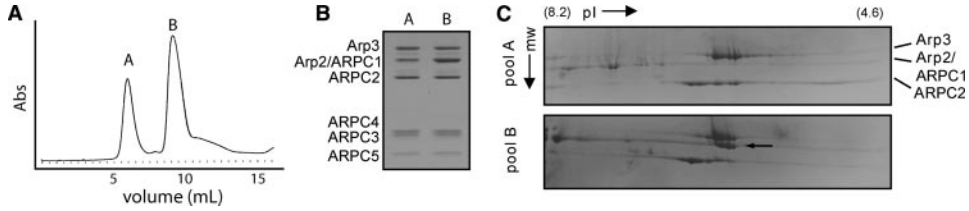

FIGURE 1. **Purification of *S. pombe* Arp2/3 complex lacking Arp2.** *A*, elution of Arp2/3 complex from a Mono Q column by a gradient of 100–400 mM NaCl. Absorbance at 280 nm shows two peaks, both containing Arp2/3 complex subunits. *B*, SDS-PAGE (10–20% gradient of acrylamide) stained with Coomassie Blue of 6.3 pmol of pools A and B from the Mono Q column further purified by gel filtration on a Superdex 200 column. ARPC1 and Arp2 are not resolved under these conditions. *C*, two-dimensional gel electrophoresis of purified pool A and pool B, stained with Coomassie Blue. Both pools contained a cluster of four spots at the apparent molecular weight of Arp3, indicating multiple species with distinct isoelectric points (the theoretical pI of Arp3 is 5.8). Pool B contained a cluster of four additional spots (*arrow*) just below Arp3, which we presumed to be Arp2 (theoretical pI = 5.8). This part of the gel shows the bands corresponding to Arp3, Arp2, ARPC1, and ARPC2. Arp2 is missing from peak A. Theoretical pI values for each subunit are as follows: Arp3, 5.8; Arp2, 5.8; ARPC1, 8.2; and ARPC2, 6.1.

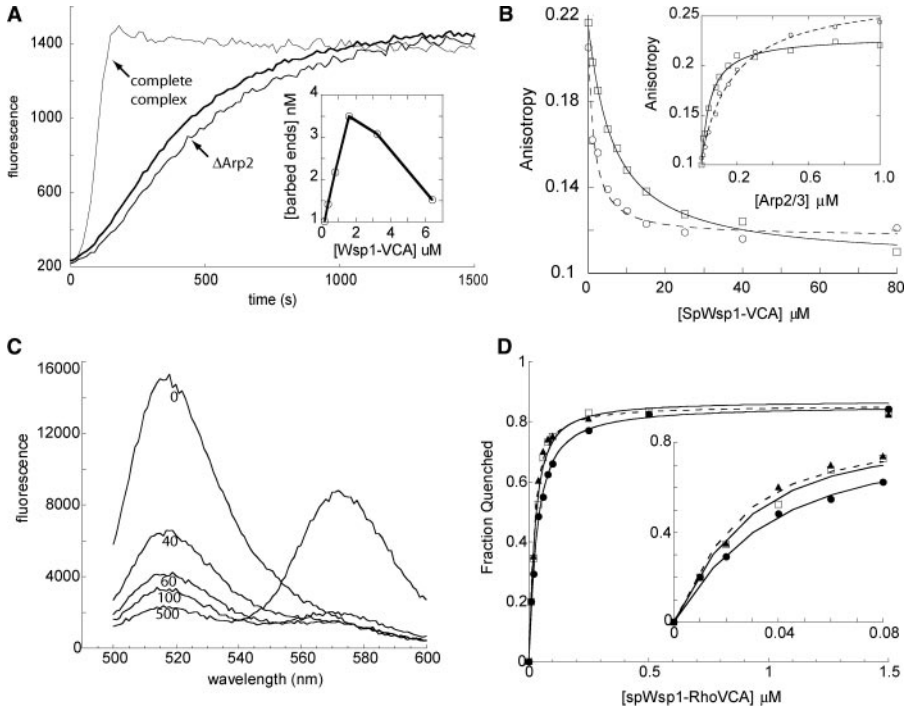

FIGURE 2. **Biochemical characterization of *S. pombe* Arp2/3 complex with and without Arp2.** *A*, effect of native and ΔArp2 Arp2/3 complex on the time course of polymerization of pyrene-labeled Mg-ATP actin. Conditions: 4 μM 15% pyrene-labeled chicken skeletal muscle actin, 0.8 μM SpWsp1-VCA, 200 μM complete SpArp2/3 complex ("complete") or ΔArp2 Arp2/3 complex ("ΔArp2") in 10 mM imidazole, pH 7.0, 50 mM KCl, 1 mM $MgCl_2$, 1 mM EGTA, 0.13 mM ATP, 63 μM $CaCl_2$, 0.3 mM DTT, 0.6 mM NaN_3 at 22 °C. *Thick black line* shows 4 μM actin and 0.8 μM SpWsp1-VCA without Arp2/3 complex. *Inset* shows the concentration of barbed ends when 50% of the actin was polymerized plotted as a function of SpWsp1-VCA concentration for the complete SpArp2/3 complex (pool B). High concentrations of VCA decrease the rate of polymer formation by inhibiting nucleation and slowing pointed end elongation (23, 44). *B*, equilibrium binding of rhodamine-labeled and unlabeled SpWsp1-VCA to ΔArp2 Arp2/3 complex and complete Arp2/3 complex measured by fluorescence anisotropy. Conditions: 50 mM KCl, 10 mM imidazole, pH 7.0, 1 mM $MgCl_2$, 1 mM EGTA, 0.1 mM ATP, 1 mM DTT, and 0.2% thesit. *Inset*: titration of 100 nM SpWsp1-Rho-VCA with ΔArp2 (*dashed line*) and native Arp2/3 complex (*solid line*). The K_d values of SpWsp1-Rho-VCA were 120 ± 13 nM for the ΔArp2 and 49 ± 5 nM for complete Arp2/3 complex. Main plot: titration of 100 nM SpWsp1-Rho-VCA and 300 nM ΔArp2 (*dashed line*) or native Arp2/3 complex (*solid line*) with unlabeled SpWsp1-VCA. Curves were fit as described in the methods giving K_d values of 0.4 ± 0.1 μM and 0.9 ± 0.1 μM for unlabeled SpWsp1-VCA binding the ΔArp2 and complete complexes, respectively. *C*, fluorescence resonance energy transfer to measure binding of SpWsp1-Rho-VCA to OG-actin. Emission scans showing the dependence of the quenching of the fluorescence of 100 nM OG-actin on the concentration of SpWsp1-Rho-VCA in the same buffer as in *B*. *Numbers* below the curves indicate Rho-VCA concentrations, in nanomolar. Samples were excited at 480 nm. *D*, effect of ΔArp2 Arp2/3 complex and native Arp2/3 complex on binding of OG-actin to Rho-VCA measured by FRET as in *C*. Plots of fraction of OG-actin emission at 517 nm quenched verses Rho-VCA concentration. Fits of the data gave a K_d of 15.5 ± 1.7 nM for Rho-VCA binding to OG-actin (*solid line*, *open squares*). In the presence of 3 μM native Arp2/3 complex (*solid line*, *filled circles*), the K_d increased to 23.9 ± 1.3 nM. In the presence of 3 μM Arp2-less complex (*dashed line*, *filled triangles*) the K_d was 12.1 ± 1.6 nM.

microscope with a 100×, 1.4 numerical aperture PlanApo lens (Olympus), and analyzed using ImageJ software (rsb.info.nih.gov/ij/). Z-series were collected in 0.6-μm steps with 200-ms sequential excitation of YFP and CFP.

RESULTS

Isolation of S. pombe Arp2/3 Complex Lacking Arp2—Arp2/3 complex from *S. pombe* purified as a single component during ammonium sulfate precipitation, ion-exchange chromatography (Q-Sepharose) and affinity chromatography on GST-N-WASp-VCA on a glutathione-Sepharose 4B column but split into two peaks during anion exchange chromatography on Mono Q. The first Mono Q peak eluted at a conductivity of 22 mS/cm, and the second peak eluted at 29 mS/cm (Fig. 1*A*). We completed the purification of the two fractions of Arp2/3 complex by gel filtration on a column of Superdex 200. Both peaks contained Arp2/3 complex subunits, but the band on SDS-PAGE previously shown to contain both Arp2 and ARPC1 (7) was less intense in pool A (Fig. 1*B*). Two-dimensional PAGE (Fig. 1*C*) showed that pool A lacked a cluster of four spots corresponding to Arp2 (theoretical pI = 5.8). Immunoblots with an *S. pombe* Arp2 antibody verified that Arp2 was missing (data not shown). The fraction of complex lacking Arp2 (ΔArp2 Arp2/3 complex) ranged from 5 to 35% (average = 13%) of total Arp2/3 complex in five preparations from wild-type cells.

Arp2 Is Required for Arp2/3 Complex Nucleation Activity—Polymerization assays showed that 200 nM ΔArp2 Arp2/3 complex did not nucleate actin filaments, whereas 200 nM of complete Arp2/3 complex (pool B) increased the concentration of barbed ends to a maximum of 3.5 nM in the presence of 1.6 μM SpWsp1-VCA and 4 μM chicken skeletal muscle actin (Fig. 2*A*). Even 1 μM ΔArp2Arp2/3 complex had no detectable nucleation activity (data not shown).

The ΔArp2 Arp2/3 Complex Binds SpWsp1-VCA and Actin Monomer—To determine the basis for the inactivity of ΔArp2 Arp2/3 complex, we used fluorescence anisotropy to measure the affinity of rhodamine-labeled SpWsp1-VCA (Rho-VCA) for complete and ΔArp2 Arp2/3 complex. Rho-VCA bound complete Arp2/3 complex with a dissociation equilibrium constant (K_d) of 49 ± 5 nM and the ΔArp2 complex with an affinity of 120 ± 13 nM (Fig. 2*B*, *inset*). Because the rhodamine label can affect the affinity of VCA for Arp2/3 complex (14), we carried out competition assays using unlabeled SpWsp1-VCA (VCA) (Fig. 2*B*). VCA had a slightly higher affinity (K_d = 0.4 ± 0.1 μM) for ΔArp2 Arp2/3 complex than native Arp2/3 complex (K_d = 0.9 ± 0.1 μM). Therefore, the Arp2-less complex is not inactive due to a loss of ability to bind this nucleation-promoting factor.

We next sought to determine if VCA bound to ΔArp2 Arp2/3 complex could recruit an actin monomer to form the ternary complex of Arp2/3 complex, NPF, and an actin monomer. This ternary complex is thought to assemble before binding to an actin filament to initiate a branch (14). To detect interaction of the VCA NPF with actin, we used fluorescence energy resonance transfer (FRET) from an Oregon Green 488 label on Cys-374 of actin (OG-actin) to Rho-VCA (Fig. 2*C*) (35). This assay gave a K_d of 16 ± 2 nM for Rho-VCA binding OG-actin in the absence of Arp2/3 complex (Fig. 2*D*). FRET was then measured in the presence of 3 μM Arp2/3 complex, so that >98% of the Rho-VCA was bound to Arp2/3 complex. The presence of 3 μM complete Arp2/3 complex slightly increased the K_d of Rho-VCA and OG-actin to 24 ± 1 nM, whereas the presence of 3 μM ΔArp2Arp2/3 complex had no effect on the binding (K_d = 12 ± 2 nM). These results indicate that both complete and ΔArp2 Arp2/3 complexes can form a ternary complex with a VCA nucleation-promoting factor and an actin monomer. Because excess Arp2/3 complex does not increase the affinity of actin for Rho-VCA, we conclude that actin does not make productive contacts with Arp2/3 complex in the ternary complex.

Structure of ΔArp2 Arp2/3 Complex—To determine whether loss of the Arp2 subunit perturbs the structure of Arp2/3 complex, we solved the crystal structure of ΔArp2Arp2/3 complex using molecular replacement with a homology model based on the crystal structure of bovine Arp2/3 complex (31) to estimate initial phases. We used this model to generate a solvent-flattened electron density map averaged using the two molecules in the asymmetric unit. The map showed density for a number of features not included in the original model, including a section of 33 residues of random coil inserted into ARPC1 and ATP in the Arp3 cleft (see "Discussion"). Three successive rounds of rebuilding and restrained refinement improved the model. Of the 1615 total residues per complex, 1308 were modeled, but 287 of these were lacking density for side chains and were modeled as alanine. Much of the backbone of ARPC3 was disordered, so only 65% of this subunit could be modeled. The final R_{free} was 34.4%, and the final R_{work} was 32.4% (Table 1), high *R*-factors typical of this resolution range. Despite the low resolution, omit electron density maps calculated at the start of the refinement clearly showed not only the secondary structure, but side-chain density for most residues (supplemental Fig. S1). This is the first crystal structure of Arp2/3 complex other than that from cow (10–12). Given the limited resolution of the data, we confine our discussion to comparisons of gross structural features of *S. pombe* and bovine complexes, such as the overall arrangement of the subunits and the conformation of long backbone segments that adopt dramatically different conformations in the structures.

TABLE 1
Data collection and refinement statistics

Data collection statistics	
Resolution limits (Å)	29.0-3.80
Space group	$P4_222$
Cell constants	a = b = 218.98 c = 315.05 α = β = γ = 90.0
Mosaicity (°)	0.46
Measured reflections	1,179,649
Unique reflections	72,502
Mean I/σ	9.5 (2.6)
R_{sym} (%)	19.8 (49.5)
Completeness (%)	99.4 (95.2)
Refinement statistics	
Modeled atoms	18,717
R_{free} reflections	3,847 (5%)
Average *B*-factor (Å^2)	74.7
Root mean square from ideal	
Bond lengths (Å)	0.007
Bond angles (°)	1.042
Ramachandran statistics	
Most favored	1,751 (76.2%)
Additionally allowed	492 (21.4%)
Generously allowed	54 (2.3%)
Disallowed	0
R_{free} (%)	34.4
R_{work} (%)	32.4

The overall structure of the ΔArp2 Arp2/3 complex from *S. pombe* closely resembles bovine Arp2/3 complex, except for the absence of Arp2 (Fig. 3*A*). Arp2/3 complexes from these two species can be overlaid with an overall root mean square deviation of 1.85 Å for 1166 aligned Cα atoms. Therefore, dissociation of Arp2 does not cause major changes in the rest of the complex (see supplemental Fig. S2 for detailed analysis).

The complete *S. pombe* Arp2/3 complex did not crystallize under the same conditions used to grow crystals of ΔArp2 Arp2/3 complex. Modeling Arp2 into the ΔArp2 Arp2/3 complex crystal revealed that Arp2 sterically clashes with the Arp3 subunit from a symmetry-related complex, explaining why the packing arrangement is not possible if Arp2 is present.

The presence of the ARPC1 insert was the most striking feature of the electron density map of *S. pombe* ΔArp2 Arp2/3 complex (Fig. 3, *A* and *B*, and 4). Electron density for this region was present in the first $F_o - F_c$ map and subsequent rounds of rebuilding/refinement allowed us to build 19 of 43 residues of the insert. This region forms a random coil that inserts into the groove between subdomains 2 and 4 of Arp3 from the other molecule in the asymmetric unit (supplemental Fig. S3*A*). In some crystals of bovine Arp2/3 complex, the most conserved portion of the ARPC1 insert forms an α-helix, which packs against the barbed end of Arp3 between subdomains 1 and 3 in a symmetry-related molecule (supplemental Fig. S3*B*) (10). The conformations of the ARPC1 inserts differ markedly in crystals of *S. pombe* and bovine Arp2/3 complexes (Fig. 3*A*). The ordered region of the insert in the structure of ΔArp2 Arp2/3 complex consists of residues unique to *S. pombe* (Fig. 3*C*), whereas the conserved region of the insert that forms an α-helix in some bovine Arp2/3 complex structures is disordered in the

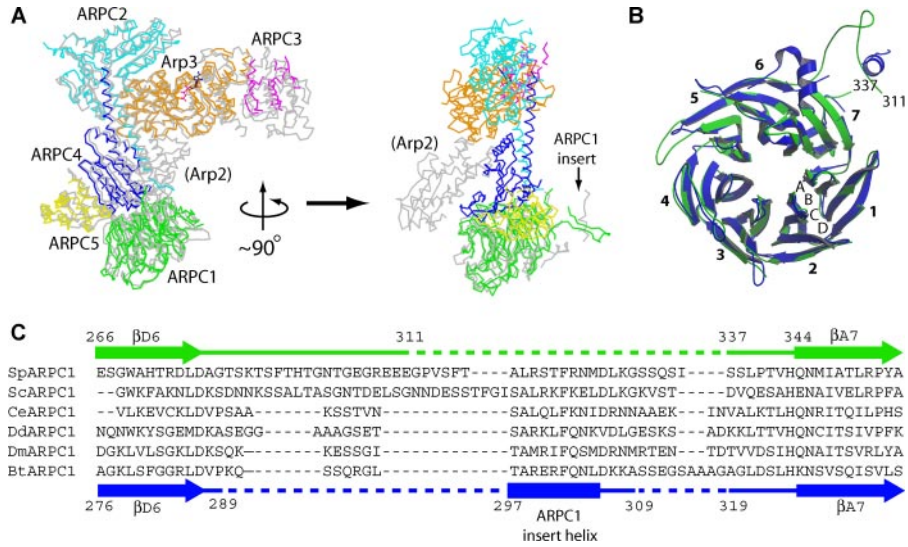

FIGURE 3. **Crystal structure of SpArp2/3 complex lacking Arp2.** *A*, Cα trace showing overlay of the ΔArp2 Arp2/3 complex (*orange*, Arp3; *green*, ARPC1; *cyan*, ARPC2; *magenta*, ARPC3; *blue*, ARPC4; *yellow*, ARPC5) onto the bovine apo-protein complex (1K8K.pdb, *gray* Cα trace). The overall arrangement of the subunits is identical in both Arp2/3 complexes with 1166 atoms overlaid with an overall root mean square deviation of 1.9 Å^2. The *left panel* shows the standard orientation of the complex, the *right panel* shows the complex rotated by 90° about the vertical axis. All but the Arp2 and ARPC1 subunits of the bovine complex are omitted from the *right panel* for clarity. *B*, *ribbon diagrams* of overlaid *S. pombe* (*green*) and bovine (*blue*) ARPC1. The seven blades of the propeller are *numbered 1–7* and the β-strands from one propeller are labeled *A–D*. The ARPC1 insert is located between βD6 and βA7. *C*, sequence alignment of the ARPC1 insert from six diverse species. Abbreviations are as follows: *Sp*, *S. pombe*; *Sc*, *S. cerevisiae*; *Bt*, *Bos taurus*; *Ce*, *Caenorhabditis elegans*; *Dd*, *Dictyostelium discoideum*; and *Dm*, *Drosophila melanogaster*. Secondary structure for *S. pombe* (*green*) and bovine complexes (*blue*) is indicated above and below the alignment, respectively. *Dashed lines* indicate regions of disorder in the structures.

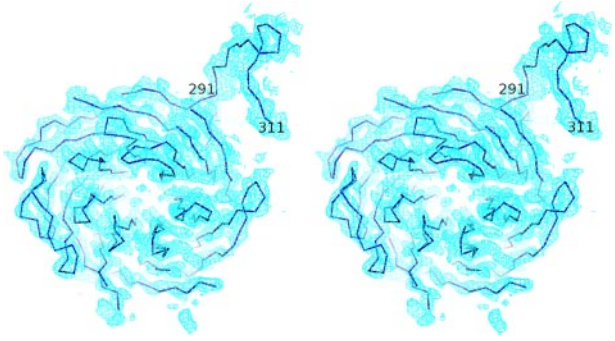

FIGURE 4. **Stereo figure of electron density of the ARPC1 insert.** $2F_o - F_c$ electron density map contoured at 2.0 σ calculated with phase contributions for the insert region from ARPC1 (subunits C and H, residues 291–311) omitted. Cα trace of ARPC1 is shown in *blue*.

structure of ΔArp2 Arp2/3 complex (Fig. 3*C*). The conserved portion of the ARPC1 insert is proposed to interact with one or more actin subunits in the mother filament (9, 10). The flexibility revealed by our new structure may be critical for this proposed function of this part of Arp2/3 complex.

The N Terminus of ARPC5 Is Not Essential for Activity—A model of Arp2/3 complex in an actin filament branch based on a three-dimensional reconstruction from electron tomograms has Arp2 positioned next to Arp3 as the second subunit in the daughter filament (9). This requires a shift of Arp2 by 31 Å from its position in the inactive conformations captured in crystals. The "migration model" for activation (22) proposed that the N terminus of ARPC5 serves as a tether for Arp2 as it dissociates from Arp3, ARPC1, and ARPC4 and migrates into the active conformation (Fig. 5, *A* and *B*).

We tested this hypothesis by mutating the conserved arginine from the N terminus of ARPC5 to a glutamic acid (ARPC5R3E) or deleting the N terminus entirely (ARPC5ΔN). Both mutant strains grew normally at 30 °C on YES plates but slower than wild type at 25 °C and 36 °C on YES + 1 M NaCl (data not shown). Additionally, both mutants were defective in expelling Phloxin-B at 25 °C and 36 °C, but not at 30 °C (data not shown). The ARPC5ΔN strain yielded ~50% more purified complex lacking Arp2 than wild-type cells (data not shown). Purified ARPC5ΔN Arp2/3 complex (Fig. 5*C*) nucleated filaments as efficiently as native *Sp*Arp2/3 complex (Fig. 5*D*). Thus, the N terminus of ARPC5 is not necessary for branching nucleation *in vitro*.

Arp2 Co-localizes with Other Arp2/3 Complex Subunits throughout the Cell Cycle—To determine if Arp2/3 complex in some parts of cells lacks Arp2, we imaged haploid strains of *S. pombe* expressing both Arp2 C-terminally labeled with cyan fluorescent protein (CFP) and ARPC3 C-terminally labeled with yellow fluorescent protein (YFP). Both tagged genes were expressed from native promoters and provided the sole copy of the gene. Cells depending on both tagged proteins were viable but often misshapen. Their actin patches turned over slower than patches in cells with only one tagged Arp.[3] Arp2 and ARPC3 co-localized in actin patches during all stages of the cell cycle (Fig. 6*A*). The relative fluorescence intensities of Arp2-CFP and ARPC3-YFP in patches were well correlated (Fig. 6*B*), showing that subpopulations of patches depleted of Arp2 were not present. The ratios of Arp2-CFP and ARPC3-YFP fluorescence were unequal in some patches moving away from the plasma membrane, owing to the time lapse between acquisition of CFP and YFP images. These results suggest that, if Arp2 dissociates from the rest of Arp2/3 complex in *S. pombe*, it does not leave the actin patches.

DISCUSSION

Isolation and Activity of the ΔArp2 Arp2/3 Complex—We considered multiple hypotheses to explain why some of purified fission yeast Arp2/3 complex lacks Arp2. Measurements of fluorescently tagged Arp2/3 complex subunits in fission yeast indicated that all subunits were present in the cytoplasm at near equal concentrations, with Arp2 the second most abundantly expressed subunit (36). Therefore, low levels of Arp2 expression cannot explain the existence of the ΔArp2 Arp2/3 complex.

[3] V. Sirotkin, personal communication.

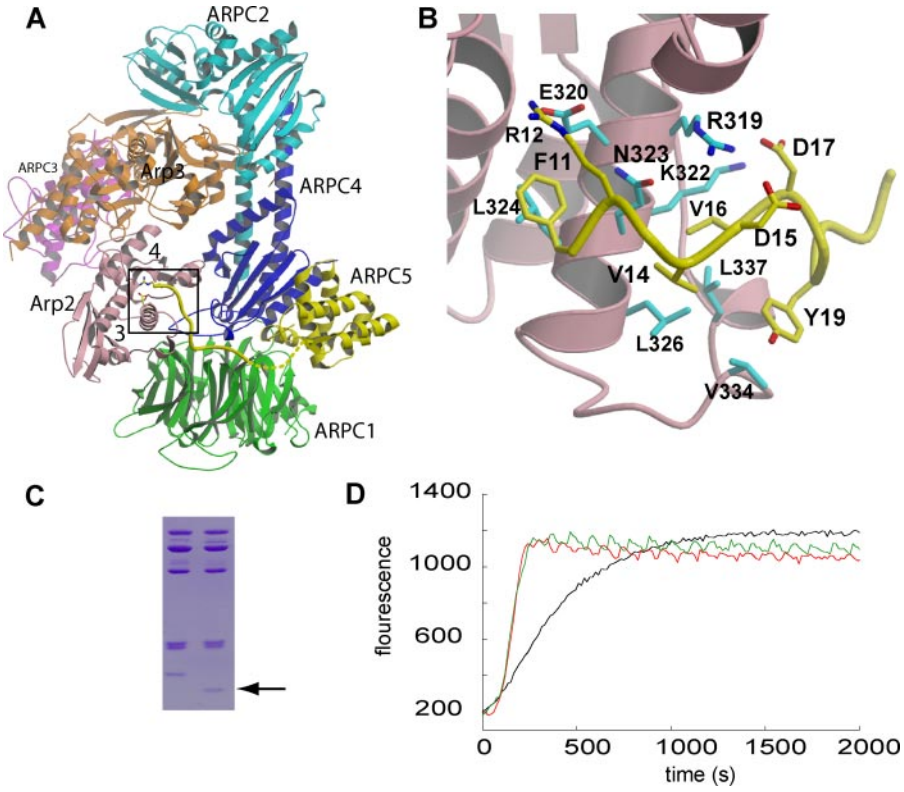

FIGURE 5. **The N-terminal residues of ARPC5 are not required for nucleation activity of purified *S. pombe* Arp2/3 complex.** *A*, ribbon diagram of bovine Arp2/3 complex (1K8K) showing the "back side" of the complex relative to the standard orientation in Fig. 3*A*. The N terminus of ARPC5 forms a random coil that wraps around the back of the complex and binds to a groove between subdomains 3 and 4 of Arp2. Disordered residues of ARPC5 (31–34) are indicated with a *dashed yellow line*. *B*, detail of the *boxed region* in *A* with key side chains shown as *sticks*. Arp2 is *pink*, and ARPC5 is *yellow*. *C*, SDS-PAGE of purified wild-type (*left lane*) and ARPC5ΔN complexes stained with Coomassie Blue. Fourteen residues are deleted from the N terminus of ARPC5ΔN Arp2/3 complex (see supplemental Fig. S4). The mutated ARPC5 subunit has a higher mobility than the native subunit (*arrow*). *D*, comparison of the effects of native and ARPC5ΔN Arp2/3 complex on the time course of the polymerization of pyrene-labeled actin. Conditions: same as those in Fig. 2*A* with 80 nM wild-type (*red*) or ARPC5ΔN (*green*) Arp2/3 complex, 1.0 μM SpWsp1-VCA, 4 μM 15% pyrene-labeled Mg-ATP actin. The *black line* shows actin polymerization in the absence of Arp2/3 complex and activator.

Dissociation of Arp2 during purification is the most likely explanation for the presence of ΔArp2 Arp2/3 complex. No information is available on the affinity of individual subunits for Arp2/3 complex in *S. pombe*, but no Arp2 dissociated from the complete fission yeast complex during gel-filtration chromatography, indicating that the complete complex is stable under these conditions. A similar experiment with *Acanthamoeba* Arp2/3 complex showed that the highest dissociation equilibrium constant for any subunit is 70 nM (37). However, ~7% of Arp2 dissociated when the complete complex was subjected to a second round of Mono Q purification. We conclude that Arp2 is the least tightly associated subunit in the *S. pombe* complex and that some Arp2 dissociates during anion-exchange chromatography and elution with high salt. Electrospray mass spectrometry after high-pressure liquid chromatography showed no mass differences for the individual subunits of the complete and Arp2Δ complexes.[4] Therefore, neither proteolysis during purification nor differences in post-translational modifications to subunits common to both complexes is responsible for dissociation of Arp2. We attempted to purify His-tagged Arp2 from the rest of the complex for reconstitution experiments but could not isolate adequate amounts of purified Arp2 under either native or denaturing conditions (data not shown).

Previous work suggested that Arp2 may not be essential in some organisms, but no one had studied the biochemical properties of Arp2/3 complex lacking Arp2. Winter *et al.* (38) found that deletion of ARP2 from *Saccharomyces cerevisiae* is not lethal, suggesting that actin might substitute for Arp2 during filament branching. However, the E316K mutation of *S. pombe* Arp2 causes dissociation of Arp2 from the complex and septation defects at 36 °C indicating the importance of Arp2 (39). Gournier *et al.* (21) expressed human Arp2/3 complex without the Arp2 subunit in insect cells, but could not isolate the Arp2Δ Arp2/3 complex.

Our preparation of fission yeast Arp2/3 complex lacking Arp2 did not nucleate actin filaments in an assay with SpWsp1-VCA and chicken skeletal muscle actin (Fig. 2*A*), so actin cannot substitute for Arp2 in the branching reaction. *S. pombe* Arp2 and chicken skeletal muscle actin are 45% identical, but many residues of Arp2 that contact ARPC4, ARPC1, or ARPC5 are different in actin. For example, the αG helix in Arp2 (residues 226–236) and the loop immediately following it (residues 237–242) make extensive contacts to ARPC4, and only four residues in this region are identical in actin and Arp2. In addition, both Arp2 and Arp3 contain an insert in the αK/β15 (Arp2 residues 320–334) loop not present in actin. In Arp2, this insert forms a major part of the interaction surface with the N terminus of ARPC5. In the model based on the reconstruction of branch junctions (9), the DNase-binding loop of Arp2 (residues 39–51) interacts with an actin subunit in the mother filament. The DNase-binding loop of Arp2 differs in sequence and is two residues longer than in actin. These differences provide a convincing structural basis for the failure of actin to substitute for Arp2 in the nucleation reaction.

The presence of Arp2/3 complex lacking Arp2 in extracts of *S. pombe* led us to wonder if dissociation of Arp2 plays a role in regulating Arp2/3 complex activity *in vivo*. The inactivity of ΔArp2 Arp2/3 complex is consistent with the observation that the E316K mutation in Arp2 causes defects in cell septation, a process thought to require Arp2/3 complex (39, 40). Fluorescence microscopy of wild-type fission yeast strains expressing Arp2-CFP and ARPC3-YFP showed that the ratio of Arp2 to ARPC3 was uniform in actin patches throughout the cell cycle

[4] S. Almo and W. Zenchek, Albert Einstein College of Medicine, personal communication.

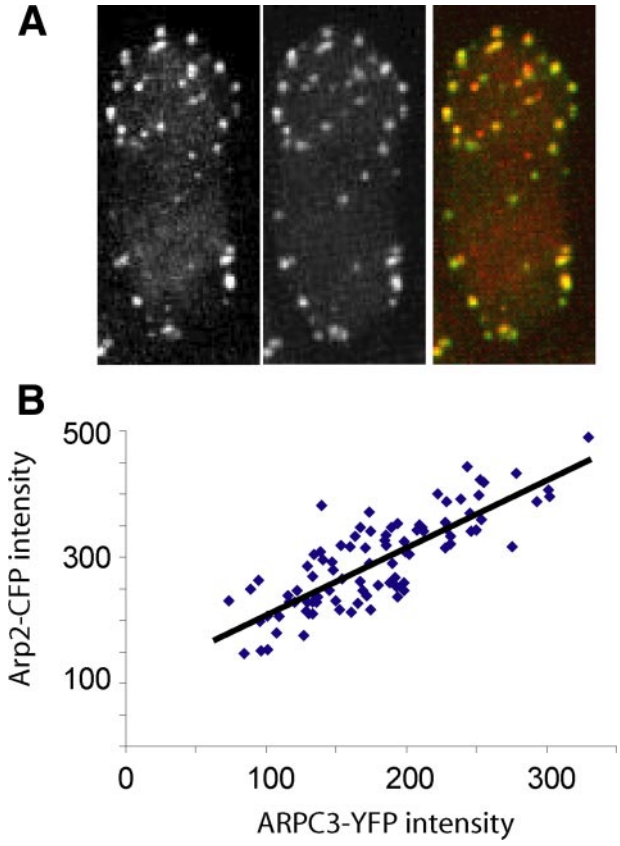

FIGURE 6. **Arp2-CFP and ARPC3-YFP co-localize to actin patches.** *A*, spinning disk confocal fluorescence micrographs of a haploid strain of *S. pombe* with Arp2 tagged on its C terminus with CFP and ARPC3 tagged on its C terminus with YFP, both expressed from their native promoters. Maximum projection images created from fourteen 0.6 μm Z-sections. *Left panel*, Arp2-CFP intensity; *center panel*, ARPC3-YFP intensity; and *right panel*, merged images with Arp2-CFP intensity shown in *red* and ARPC3-YFP intensity shown in *green*. *B*, correlation of the intensity of CFP and YFP fluorescence in individual actin patches. Plot of mean CFP and YFP intensity for 163 patches in 3 cells. The linear correlation coefficient = 0.81.

(Fig. 6). Previous studies established that all actin patches contain a 1:1:1:1:1 ratio of all five subunits measured (Arp3, Arp2, ARPC1, ARPC3, and ARPC5) (36).[3] Although we cannot rule out the possibility that Arp2 dissociates from the rest of the complex but remains in the patches, this scenario seems unlikely, because the E316K mutation, which favors dissociation of Arp2 from the complex *in vivo*, causes Arp2 to leave the actin patches and adopt a diffuse localization (39). Therefore, we have no evidence that cells use ΔArp2 Arp2/3 complex selectively in patches or other structures.

Interaction of VCA and Actin Monomers with Arp2/3 Complex Lacking Arp2—We found that the loss of Arp2 does not decrease the affinity of SpWsp1-Rho-VCA for SpArp2/3 complex. Similarly, GST-Bee1-VCA (a budding yeast WASp homolog construct) pulled down similar amounts of Arp3 from extracts of wild-type and Δ*arp2* strains of budding yeast (41). This is consistent with experiments that showed that most of the binding energy of GST-Bee1-VCA for ScArp2/3 complex comes from its interaction with the ARPC1 (Arc40) subunit (41). On the other hand, VCA constructs protect Arp2 of bovine Arp2/3 complex from oxidation in synchrotron radiation footprinting experiments (16) and have been chemically cross-linked to the Arp2 subunit of Arp2/3 complex from multiple species (17–19). All of these observations may be reconciled, if VCA contacts Arp2 without contributing strongly to the binding affinity.

Our FRET assays confirmed that the affinity of OG-actin for rhodamine-VCA is slightly weaker in the presence of the full Arp2/3 complex (K_d = 16 ± 2 nM without Arp2/3 complex, 24 ± 1 nM with Arp2/3 complex) (35). This indicates that VCA, actin, and Arp2/3 complex can interact simultaneously, but that the actin monomer in this ternary complex does not make productive contacts with Arp2/3 complex. We suggest that actin in the ternary complex must reorient relative to Arp2/3 complex subunits during the activation step (35) to establish a nucleus for the polymerization of the daughter filament. The lower affinity of actin for VCA in the presence of Arp2/3 complex also suggests that actin and Arp2/3 complex compete for a common binding site on VCA. The C region is the best candidate for this common site (14), because it binds weakly to both actin (K_d = 12 μM) and Arp2/3 complex (K_d > 200 μM) in a mutually exclusive manner (42).

The FRET assay showed that the affinity of VCA for OG-actin is 2-fold stronger (K_d = 12 ± 2 nM) with ΔArp2 Arp2/3 than full Arp2/3 complex (K_d = 24 ± 1 nM). We speculate that dissociation of Arp2 either relieves steric inhibition that prevents the C region from interacting with actin and/or that Arp2 subunit completes with actin directly by weakly binding the C region.

We note that our results differ from the interpretation of a small angle x-ray scattering model of Arp2/3 with bound activator and monomeric actin (20), in which the C-region of the activator makes extensive interactions with Arp2. Although we do not rule out weak interactions between Arp2 and the activator, our data show that the loss of Arp2 increases the affinity of VCA for Arp2/3 complex and does not affect recruitment of actin to VCA bound to Arp2/3 complex.

Insights into the Mechanism of Arp2/3 Complex Activation—Our structure of the ΔArp2 Arp2/3 complex shows that dissociation of the Arp2 subunit did not perturb the remaining subunits in the complex. This establishes the feasibility that Arp2 partially dissociates during the conformational change that activates the complex (9). However, the N terminus of ARPC5, which has been proposed to tether Arp2 to the complex during the proposed conformational rearrangement (22), is not necessary for Arp2/3 complex activity *in vitro*, suggesting that Arp2 maintains contacts with other subunits during activation. This observation supports a model where a twisting motion rotates a rigid body composed of Arp2, ARPC1, ARPC4, and ARPC5 into the active conformation (10). The interpretation of small angle x-ray scattering from Arp2/3 complex with bound activator and actin monomer also supports the rotation model (20).

Although the N-terminal tether of ARPC5 does not play a fundamental role in the activation of Arp2/3 complex, it may be important in stabilizing interactions of Arp2 with the rest of the complex. Consistent with this hypothesis, we recovered more ΔArp2 Arp2/3 complex from the ARPC5ΔN strain than wild-type cells. The residues involved in the interface between ARPC5 and Arp2 are conserved in most species (supplemental Fig. S4), but in most plant species the N terminus of ARPC5 is

too short to reach Arp2 in models based on structures of inactive bovine Arp2/3 complex (10–12) or the model of the branch junction based on electron tomography (9). Therefore, the stabilizing function of the N terminus of ARPC5 is unlikely to occur in plants.

We were surprised that Arp2 does not contribute to the affinity of VCA for Arp2/3 complex and that, in fact, the affinity is slightly higher without Arp2. This observation suggests that VCA facilitates the movement of Arp2 next to Arp3 without strongly interacting with Arp2 Perhaps Arp2 is a passive participant in activation, with interactions of other subunits of Arp2/3 complex with NPFs and a mother filament providing most of the free energy for the conformational change that creates a favorable binding site for the first actin subunit of the daughter filament with Arp2 and Arp3. Alternatively, VCA may interact strongly with Arp2 only after the complex is bound to mother filament. Consistent with this hypothesis, kinetic and thermodynamic data demonstrated multiple modes of NPF binding to Arp2/3 complex (42), and sequence similarities between C and V regions suggest that the C region may interact with Arp2 just as V interacts with actin during activation (43). Elucidation of this complex activation mechanism will require much more structural, biophysical, and biochemical information than is currently available.

Acknowledgments—We thank Kathleen Gould for the S. pombe Arp2 antibody, Chris Beltzner for yeast strains with Arp2 and Arp3 tagged with CFP and YFP, Vladimir Sirotkin for help with microscopy, Aaron Downs for help with 2D gels, Yong Xiong for advice on analyzing low resolution data, Hongli Chen for assistance with protein preparations, Aditya Paul for comments on the manuscript, and Shih-Chieh Ti and Julien Berro for deriving the formula for fitting the competition binding curve.

REFERENCES

1. Pollard, T. D., Blanchoin, L., and Mullins, R. D. (2000) *Annu. Rev. Biophys. Biomol. Struct.* **29,** 545–576
2. Pollard, T. D. (2007) *Annu. Rev. Biophys. Biomol. Struct.* **36,** 451–477
3. Chang, F., Drubin, D., and Nurse, P. (1997) *J. Cell Biol.* **137,** 169–182
4. Feierbach, B., and Chang, F. (2001) *Curr. Biol.* **11,** 1656–1665
5. McCollum, D., Feoktistova, A., Morphew, M., Balasubramanian, M., and Gould, K. L. (1996) *EMBO J.* **15,** 6438–6446
6. Toshima, J. Y., Toshima, J., Kaksonen, M., Martin, A. C., King, D. S., and Drubin, D. G. (2006) *Proc. Natl. Acad. Sci. U. S. A.* **103,** 5793–5798
7. Sirotkin, V., Beltzner, C. C., Marchand, J. B., and Pollard, T. D. (2005) *J. Cell Biol.* **170,** 637–648
8. Amann, K. J., and Pollard, T. D. (2001) *Nat. Cell Biol.* **3,** 306–310
9. Rouiller, I., Xu, X. P., Amann, K. J., Egile, C., Nickell, S., Nicastro, D., Li, R., Pollard, T. D., Volkmann, N., and Hanein, D. (2008) *J. Cell Biol.* **180,** 887–895
10. Robinson, R. C., Turbedsky, K., Kaiser, D. A., Marchand, J. B., Higgs, H. N., Choe, S., and Pollard, T. D. (2001) *Science* **294,** 1679–1684
11. Nolen, B. J., Littlefield, R. S., and Pollard, T. D. (2004) *Proc. Natl. Acad. Sci. U. S. A.* **101,** 15627–15632
12. Nolen, B. J., and Pollard, T. D. (2007) *Mol. Cell* **26,** 449–457
13. Chereau, D., Kerff, F., Graceffa, P., Grabarek, Z., Langsetmo, K., and Dominguez, R. (2005) *Proc. Natl. Acad. Sci. U. S. A.* **102,** 16644–16649
14. Marchand, J. B., Kaiser, D. A., Pollard, T. D., and Higgs, H. N. (2001) *Nat. Cell Biol.* **3,** 76–82
15. Panchal, S. C., Kaiser, D. A., Torres, E., Pollard, T. D., and Rosen, M. K. (2003) *Nat. Struct. Biol.* **10,** 591–598
16. Kiselar, J. G., Mahaffy, R., Pollard, T. D., Almo, S. C., and Chance, M. R. (2007) *Proc. Natl. Acad. Sci. U. S. A.* **104,** 1552–1557
17. Kreishman-Deitrick, M., Goley, E. D., Burdine, L., Denison, C., Egile, C., Li, R., Murali, N., Kodadek, T. J., Welch, M. D., and Rosen, M. K. (2005) *Biochemistry* **44,** 15247–15256
18. Zalevsky, J., Grigorova, I., and Mullins, R. D. (2001) *J. Biol. Chem.* **276,** 3468–3475
19. Zalevsky, J., Lempert, L., Kranitz, H., and Mullins, R. D. (2001) *Curr. Biol.* **11,** 1903–1913
20. Boczkowska, M., Rebowski, G., Petoukhov, M. V., Hayes, D. B., Svergun, D. I., and Dominguez, R. (2008) *Structure* **16,** 695–704
21. Gournier, H., Goley, E. D., Niederstrasser, H., Trinh, T., and Welch, M. D. (2001) *Mol. Cell* **8,** 1041–1052
22. Irobi, E., Aguda, A. H., Larsson, M., Guerin, C., Yin, H. L., Burtnick, L. D., Blanchoin, L., and Robinson, R. C. (2004) *EMBO J.* **23,** 3599–3608
23. Higgs, H. N., Blanchoin, L., and Pollard, T. D. (1999) *Biochemistry* **38,** 15212–15222
24. Gill, S. C., and von Hippel, P. H. (1989) *Anal. Biochem.* **182,** 319–326
25. Kapust, R. B., Tozser, J., Fox, J. D., Anderson, D. E., Cherry, S., Copeland, T. D., and Waugh, D. S. (2001) *Protein Eng.* **14,** 993–1000
26. MacLean-Fletcher, S., and Pollard, T. D. (1980) *Biochem. Biophys. Res. Commun.* **96,** 18–27
27. Pollard, T. D. (1984) *J. Cell Biol.* **99,** 769–777
28. Kuhn, J. R., and Pollard, T. D. (2005) *Biophys. J.* **88,** 1387–1402
29. Bahler, J., Wu, J. Q., Longtine, M. S., Shah, N. G., McKenzie, A., 3rd, Steever, A. B., Wach, A., Philippsen, P., and Pringle, J. R. (1998) *Yeast* **14,** 943–951
30. Keeney, J. B., and Boeke, J. D. (1994) *Genetics* **136,** 849–856
31. Beltzner, C. C., and Pollard, T. D. (2004) *J. Mol. Biol.* **336,** 551–565
32. McCoy, A. J., Grosse-Kunstleve, R. W., Adams, P. D., Winn, L. C., Storoni, L. C., and Read, R. J. (2007) *J. Appl. Crystallogr.* **40,** 658–674
33. Winn, M. D., Isupov, M. N., and Murshudov, G. N. (2001) *Acta Crystallogr. D. Biol. Crystallogr.* **57,** 122–133
34. Wu, J. Q., Kuhn, J. R., Kovar, D. R., and Pollard, T. D. (2003) *Dev. Cell* **5,** 723–734
35. Beltzner, C. C., and Pollard, T. D. (2007) *J. Biol. Chem.* **283,** 7135–7144
36. Wu, J. Q., and Pollard, T. D. (2005) *Science* **310,** 310–314
37. Mullins, R. D., Stafford, W. F., and Pollard, T. D. (1997) *J. Cell Biol.* **136,** 331–343
38. Winter, D. C., Choe, E. Y., and Li, R. (1999) *Proc. Natl. Acad. Sci. U. S. A.* **96,** 7288–7293
39. Morrell, J. L., Morphew, M., and Gould, K. L. (1999) *Mol. Biol. Cell* **10,** 4201–4215
40. Welch, M. D., Holtzman, D. A., and Drubin, D. G. (1994) *Curr. Opin. Cell Biol.* **6,** 110–119
41. Pan, F., Egile, C., Lipkin, T., and Li, R. (2004) *J. Biol. Chem.* **279,** 54629–54636
42. Kelly, A. E., Kranitz, H., Dotsch, V., and Mullins, R. D. (2006) *J. Biol. Chem.* **281,** 10589–10597
43. Aguda, A. H., Burtnick, L. D., and Robinson, R. C. (2005) *EMBO Rep.* **6,** 220–226
44. Boujemaa-Paterski, R., Gouin, E., Hansen, G., Samarin, S., Le Clainche, C., Didry, D., Dehoux, P., Cossart, P., Kocks, C., Carlier, M. F., and Pantaloni, D. (2001) *Biochemistry* **40,** 11390–11404